INFLUENCE OF THE HYDRAULIC SYSTEM LAYOUT ON THE STABILITY OF A MIXED ISLANDED POWER NETWORK

Influence de l'agencement du système hydraulique sur la stabilité d'un réseau électrique ilôté

Christian Landry[1]
christian.landry@epfl.ch

Christophe Nicolet
christophe.nicolet@powervision-eng.ch

Silvio Giacomini
silvio.giacomini@epfl.ch

François Avellan
Francois.Avellan@epfl.ch

Phone: +41 (0)21 693 2515, Fax: +41 (0)21 693 3554

KEY WORDS

Stability analysis, Pump-turbine, Modeling, Power Network, Simulation

ABSTRACT

Numerical simulation and stability analysis of an islanded power network comprising 40 MW of hydropower, 20 MW of wind power and 60 MW of gas-fired power plant are investigated. First, the modeling of each power plant is fully described. The wind farm is modeled through an aggregated model approach of 10 wind turbines of 2 MW and comprises a stochastic model of wind evolution with wind gust. The hydraulic power plant comprises the upstream reservoir, a 1000 meters gallery, a surge tank, the 500 meters long penstock feeding a low specific speed pump-turbine and connected to the downstream tank through a 70 meters long tailrace water tunnel. The model of gas-fired power plant includes an upstream rotating compressor coupled to a downstream turbine, and a combustion chamber in-between. To predict the performance of the gas turbine engine, both at design and off-design conditions, performance maps are integrated in the modeling.

Then, the capability of the hydraulic power plant to compensate wind power variations or load rejections is investigated using the EPFL simulation software SIMSEN to perform time domain simulation of the entire mixed islanded power network. This study shows the evolution of the response time of the hydraulic part as function of the penstock length and highlights the influence of the hydraulic layout on the power system stability. The dynamic performances of such hydraulic power plants are of highest interest for improving stability of mixed islanded power network, but require reliable simulation model of the entire network for safety and optimization purposes.

1. INTRODUCTION

---

[1] Corresponding author

Electricity generated from intermittent energy resources is developing rapidly worldwide. Earlier studies have found that energy storage can compensate for the stochastic nature of the variable energy sources by storing the excessive energy when generation exceeds predicted levels and providing it back to the grid when generation levels fall short. For instance, islanded power networks featuring high level of wind power penetration are subjected to undesired perturbation jeopardizing the power network stability [1]. Consequently, pumped storage plants are a proven solution for storing electricity at large scale and offering flexibility to the power management. The high dynamic performances of such pumped storage plants are of highest interest for improving stability of mixed islanded power network, but require reliable simulation model of the entire power network for safety and optimization purposes [2].

This paper presents the modeling, numerical simulations and stability analysis of an islanded power network comprising 40 MW of hydropower, 20 MW of wind power and 60 MW of gas-fired power plant. First, the modeling of each power plant is fully described. The wind farm is modeled through an aggregated model approach of 10 wind turbines of 2 MW and comprises a stochastic model of wind evolution with wind gust. The hydraulic power plant comprises the upstream reservoir, a 1000 meters gallery, a surge tank, the 500 meters long penstock feeding a low specific speed pump-turbine ($v = 0.217$) and connected to the downstream tank through a 70 meters long tailrace water tunnel. The model of gas-fired power plant includes an upstream rotating compressor coupled to a downstream turbine, and a combustion chamber in-between. To predict the performance of the gas turbine engine, both at design and off-design conditions, performance maps are integrated in the modeling.

The power plants are connected to a passive consumer load via a 500 kV electrical network. Then, the capability of the hydraulic power plant to compensate wind power variations or load rejections is investigated using the EPFL simulation software SIMSEN to perform time domain simulation of the entire mixed islanded power network. This study shows the evolution of the response time of the hydraulic part as function of the penstock length and highlights the influence of the hydraulic layout on the power system stability.

2. MODELING OF HYDRAULIC POWER PLANT

The modeling of the hydraulic components based on equivalent scheme representation is presented in this section. The following set of hyperbolic partial differential equations describes the one-dimensional momentum and continuity balances for an elementary pipe of length dx and wave speed a. Moreover, we assume uniform pressure and velocity distributions in the cross section A and we neglect the convective terms [3].

$$\begin{cases} \dfrac{\partial h}{\partial t} + \dfrac{a^2}{gA} \cdot \dfrac{\partial Q}{\partial x} = 0 \\ \dfrac{\partial h}{\partial x} + \dfrac{1}{gA} \cdot \dfrac{\partial Q}{\partial t} + \dfrac{\lambda |Q|}{2gDA^2} \cdot Q = 0 \end{cases} \tag{1}$$

The system (1) is solved using the Finite Difference Method with 1st order centered scheme discretization in space and a scheme of Lax for the discharge variable. This discretization leads to a system of ordinary differential equations that can be represented as a T-shaped equivalent scheme [4] as presented in Figure 1.
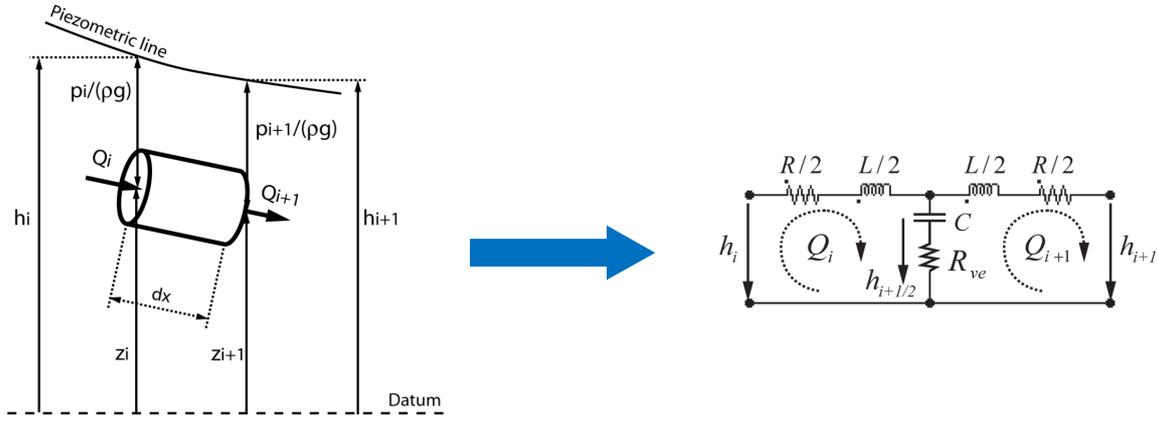
Figure 1: Representation of an elementary hydraulic pipe of length *dx* and its equivalent circuit

The RLC parameters of the equivalent scheme are given by:

$$R = \frac{\lambda \, |\overline{Q}| \, dx}{2gDA^2}, \quad L = \frac{dx}{gA}, \quad C = \frac{gAdx}{a^2}, \quad (2)$$

where λ is the local loss coefficient and D is the diameter of the elementary pipe. The hydraulic resistance R, the hydraulic inductance L and the hydraulic capacitance C correspond respectively to energy losses, inertia and storage effects. Moreover, in order to predict accurately pressure fluctuation amplitudes and system stability, it is necessary to take into account the viscoelastic behavior due to energy dissipation during the wall deflection. This additional dissipation leads to a resistance in series with the capacitance. This viscoelastic resistance is accounting for both fluid and pipe material viscoelasticity and can be expressed as:

$$R_{ve} = \frac{\mu_{equ}}{A \rho g dx} \quad (3)$$

with μ_{equ} the equivalent viscoelastic damping of both the fluid and the wall. The model of a pipe with a length L is made of a series of elements based on the equivalent scheme illustrated in Figure 1, the system of equations being set up using Kirchhoff laws. This modeling approach based on equivalent electrical schemes of hydraulic components is extended to all the standard hydraulic components such as valves, surge tanks, air vessels, cavitation development, Francis pump-turbines, Kaplan turbines, pumps, etc. and provides a high level of abstraction allowing for a rigorous formalism. This modeling approach is also extended to all electrical components such as transmission lines, transformers, synchronous machines, etc. Finally, models of all those components are implemented in the EPFL software SIMSEN, developed for the simulation of the dynamic behavior of hydroelectric power plants [5].

The layout of the hydraulic power plant is presented in Figure 2. In this case study, the influence of two different penstocks will be highlighted: a 500 meters short penstock and a 2000 meters long penstock. The power plant is constituted of an upstream reservoir, a 1000 meters long gallery, a short or a long penstock connected to a 40 MW pump-turbine. Moreover, the hydraulic machine is connected to the downstream reservoir by a tailrace water tunnel of 70 meters long. Finally, the turbine is equipped with a PID turbine speed governor including a rate limiter and the generator is controlled by ABB Unitrol voltage regulator. Table 1 gives the main characteristics of the hydraulic power plant.
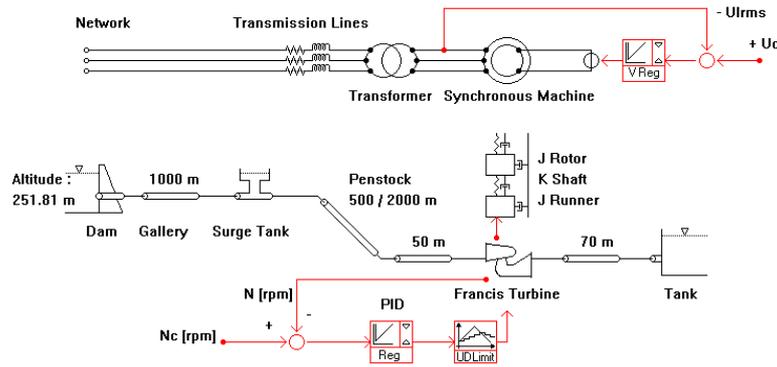
Figure 2: Hydraulic power plant model

Table 1: Hydraulic Power Plant characteristics

Gallery				Penstock			
Length:	L_G	= 1'000	m	Length:	L_p	= 500/1000	m
Diameter:	D_G	= 3	m	Diameter:	D_p	= 2.02/2.64	m
Wave speed:	a_G	= 1'200	m/s	Wave speed:	a_p	= 1'200	m/s
Francis turbine				**Generator**			
Rated mechanical power:	P_r	= 40	MW	Rated apparent power:	S_n	= 42.88	MVA
Rated speed:	N_r	= 500	rpm	Rated phase to phase voltage:	V_n	= 17.5	kV
Rated discharge:	Q_r	= 17.7	m³/s	Frequency:	f	= 50	Hz
Rated head:	H_r	= 242	m	Inertia:	J_t	= 10^5	kg·m²
Specific speed:	ν	= 0.217		Number of poles pairs:	P	= 6	
Reference diameter:	D_{ref}	= 2.6	m	Stator windings:	Y		
Surge Tank				**Coupling shaft**			
Mid tank section:	A_{st}	= 15	m²	Stiffness:	K	= 10^8	Nm/rad
				Viscous damping:	μ	= 10^3	Nm·s/rad

For completeness, the electrical system of the hydraulic power plant model is a synchronous machine of 43 MVA and is connected to the islanded network through 17.5/500-kV Yd5 transformers. The synchronous machine is laminated rotor type and is modeled according to a model with transient and subtransient characteristic quantities.

3. MODELING OF THE WIND FARM

The model of a 2MW wind turbine is presented in Figure 3. The turbine can adjust the blade pitch angle θ to provide the highest power coefficient for different tip ratio $U_t / C_{\inf}$, where U_t is the blade tip velocity and $C_{\inf}$ is the wind velocity. But, for tip speed ratio below 8, the pitch angle is selected to generate the 2 MW output power limit. Finally, the characteristic of the shaft stiffness, the gear box and the synchronous generator of 2 MVA with voltage regulator are given in Table 2.
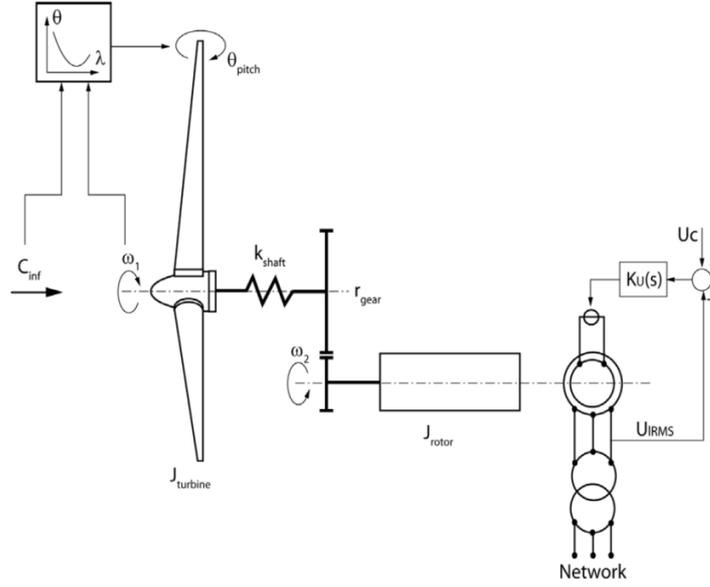
Figure 3: Wind turbine model

Table 2: Wind turbine characteristics

Wind Turbine				Generator			
Number of blades:	N_b	= 3		Rated apparent power:	S_n	= 2.2	MVA
Diameter:	D_W	= 75	m	Rated phase to phase voltage:	V_n	= 400	V
Rotational speed:	n_W	= 24.75	rpm	Frequency:	f	= 50	Hz
Inertia:	J_W	= $3.15 \cdot 10^6$	kg·m^2	Inertia:	J_{GW}	= $6.48 \cdot 10^4$	kg·m^2
				Number of poles pairs:	P	= 40	
				Stator windings:	Y		
Operating Data				**Coupling shaft**			
Cut-in wind velocity:	$C_{cut\text{-}in}$	= 3.5	m/s	Stiffness:	k_{shaft}	= $2.2 \cdot 10^8$	Nm/rad
Cut-out wind velocity:	$C_{cut\text{-}out}$	= 20	m/s	Viscous damping:	μ_W	= $5 \cdot 10^5$	Nm·s/rad
Rated wind velocity:	C_w	= 13	m/s	Gear ratio:	r_{gear}	= 3.032	

The turbulent wind model is composed of a wind mean value and a wind gust, as suggested by Slootweg *et al.* [6]. The turbulent gust is modeled by a Pseudo-Random-Binary-sequence, PRBS, obtained by a shift register method, see [7]. The mechanical power P transmitted by the fluid to the wind turbine can be expressed as :

$$P = \frac{1}{2}\rho A_{ref} C_p\left(\lambda,\theta\right) \cdot C_{\inf}^3 \qquad (4)$$

Where A_{ref} is the swept area, C_p is the power coefficient, ρ is the air density and λ is the tip speed ratio given by:

$$\lambda = \frac{U_t}{C_{\inf}} = \frac{D_w \omega}{C_{\inf}} \qquad (5)$$

For power grid stability purposes, it is possible to use an aggregated wind farm model, consisting of one wind turbine equivalent to *n* single wind turbines as presented in Figure 4. Then, according to the energy conservation and in order to keep the same torsional mode eigenfrequency, the active power P_n, rotating inertias J, the shaft stiffness k_{shaft}, and the swept area A_{ref}, are multiplied by the number of wind turbine *n*.

For completeness, the electrical system of the aggregated wind farm model is a synchronous machine of 22 MVA and is connected to the islanded network through 400/500-kV Yd5 transformers. The synchronous

machine is laminated rotor type and is modeled according to a model with transient and subtransient characteristic quantities.

10 x 2 MW   =   1 x 20 MW
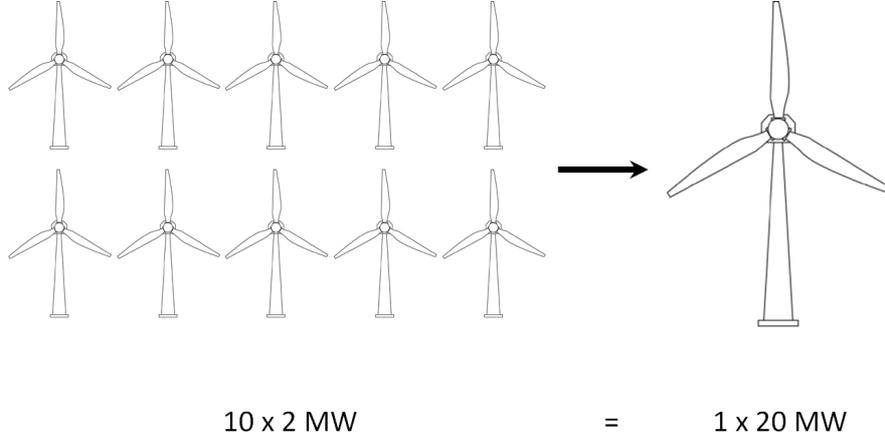
Figure 4: Wind turbine farm of 10 x 2 MW modeled as an equivalent wind turbine of 20 MW

4. MODELING OF GAS-FIRED POWER PLANT

The gas turbine engine is a complex assembly of a variety of components that are designed on the basis of thermodynamic laws. The design and operation theories of these individual components are complicated. Therefore, to simplify the modeling, the following assumptions are taken into account:

i.   The compressor shaft speed N_c equals the turbine shaft speed N_t,

$$N_c = N_t = N \tag{6}$$

ii.   The gas mass flow through turbine m_g is the sum of the air mass flow through compressor m_a and the fuel mass flow m_f,

$$m_g = m_a + m_f \tag{7}$$

iii. We assume that the pressure loss in the combustion chamber is a constant small percentage ξ_{cc} of the combustion chamber inlet pressure P_{02},

$$P_{03} = \left(1 - \xi_{cc}\right) P_{02} \tag{8}$$

iv.   We assume that the pressure loss in the compressor inlet is a constant small percentage ξ_c of the atmospheric pressure.

$$P_{04} = \left(1 - \xi_c\right) P_{02} \cong P_{01} \tag{9}$$

v.   The fuel was assumed to be pure methane and the combustion model was taken from Keating [11] and Turns [12], considering a complete combustion of the fuel without dissociation.
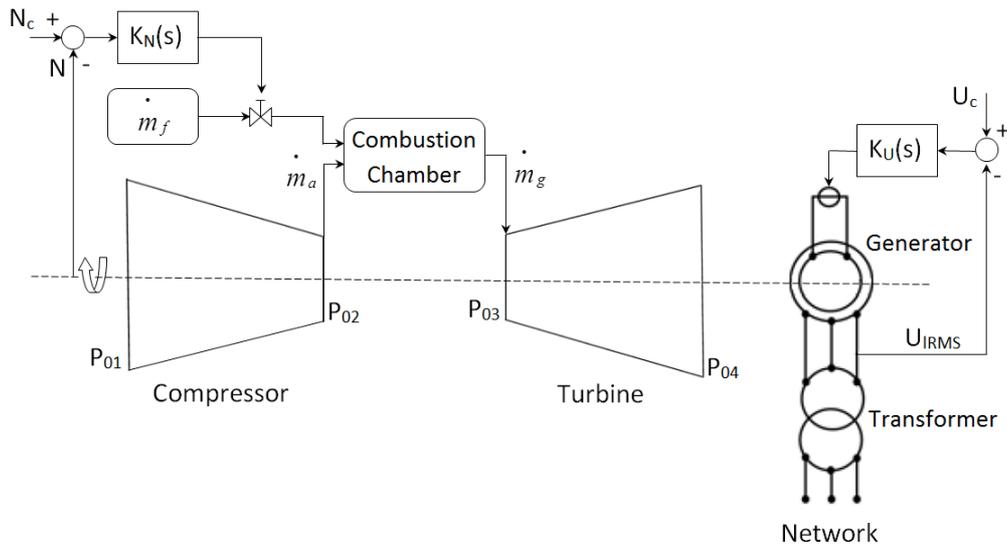
Figure 5: Gas-fired turbine model

Moreover, the gas turbine design and off-design model presented in this paper aims both at computational simplicity and at the ability to deal with plants having large variations in the operating parameters. Thus, some tools were needed to predict the performance of gas turbine engines especially at off design conditions where its performance was significantly affected by the load and the operating conditions.

A solution to define the off-design behavior of the compressor and turbine is to use performance maps for each gas turbine component. Starting from known maps, such as those shown in Figure 6, the evaluation of the off-design performance of different gas turbines can be investigated.
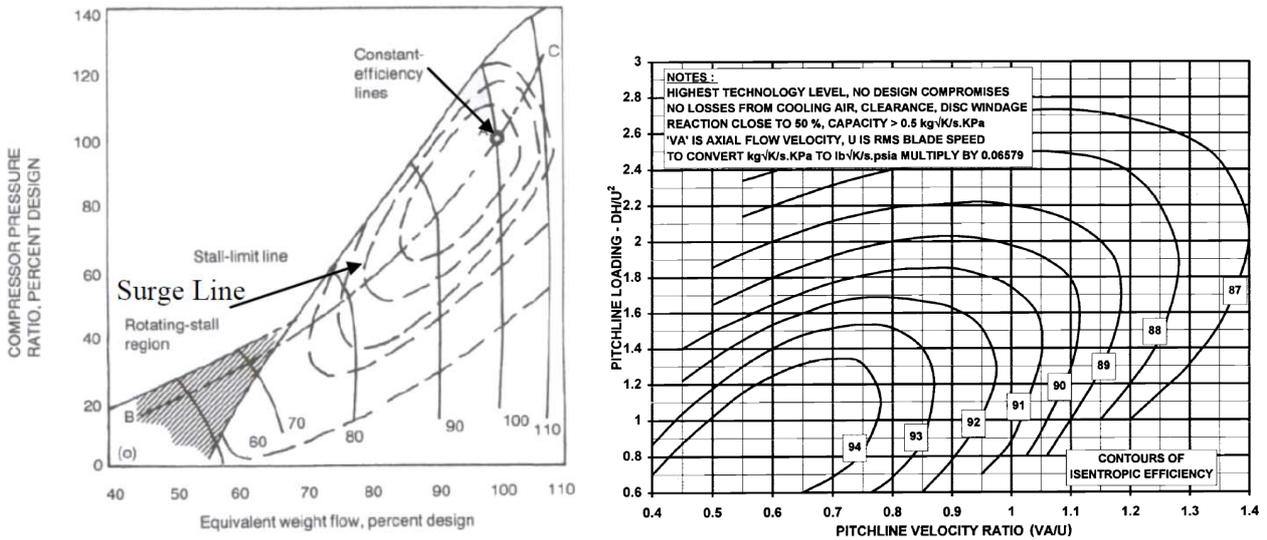
**Figure 6**: Performance maps of a compressor (left) [8] and a turbine (right) [9]

For completeness, the electrical system of the gas-fired power plant model is a synchronous machine of 66.6 MVA and is connected to the islanded network through 17.5/500-kV Yd5 transformers. The synchronous machine is solid iron rotor type. Finally, Table 3 gives the main characteristics of the gas-fired power plant.

Table 3: Gas-fired power plant characteristics

Compressor				Turbine			
Specific heat capacity:	$C_{p,c}$	= 1004	J/kg·K	Specific heat capacity:	$C_{p,T}$	= 1156	J/kg·K
Individual Gas constant:	R	= 287	J/kg·K	Individual Gas constant:	R	= 287	J/kg·K
Specific Heat Ratio:	K_c	= 1.4		Specific Heat Ratio:	K_T	= 1.35	
Pressure Ratio (Nominal):	$\pi_{c,nom}$	= 20		Rotational speed:	N_T	= 1500	rpm
Rotational speed:	N_c	= 1500	rpm	Inertia:	J_T	= $3.16\cdot10^5$	kg·m²
Inertia:	J_c	= $2.4\cdot10^4$	kg·m²				
Gas-fired Turbine				**Generator**			
Power	P	= 60	MW	Rated apparent power:	S_n	= 66.6	MVA
Efficiency	η_{nom}	= 37	%	Rated phase to phase voltage:	V_n	= 17.5	kV
Exhaust gas flow	Q_{ex}	= 182.3	kg/s	Frequency:	f	= 50	Hz
Exhaust gas temperature	T_{ex}	= 480	°C	Inertia:	J_{GT}	= $1\cdot10^4$	kg·m²
				Number of poles pairs:	P	= 2	
				Stator windings:	Y		

5. TRANSIENT BEHAVIOR OF MIXED ISLANDED POWER NETWORK

The full SIMSEN model of the mixed power network is presented in Figure 8 based on the hydraulic, gas-fired and wind power plant models described above. The model includes the 500 kV transmission lines and the passive consumer load. Moreover, in order to make the system behavior more realistic, response times of the power plants are modeled. Figure 7 compares the adjustable load rates of several types of power plants. Overall, general hydro plants have the fastest response times, able to change from full power to zero and vice versa within one minute. However, coal thermal power plants respond comparatively slowly [10].
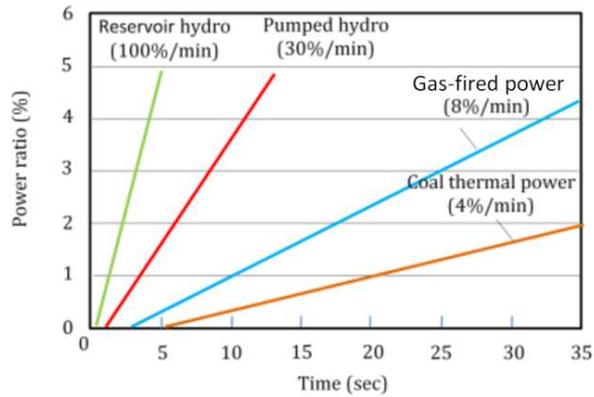
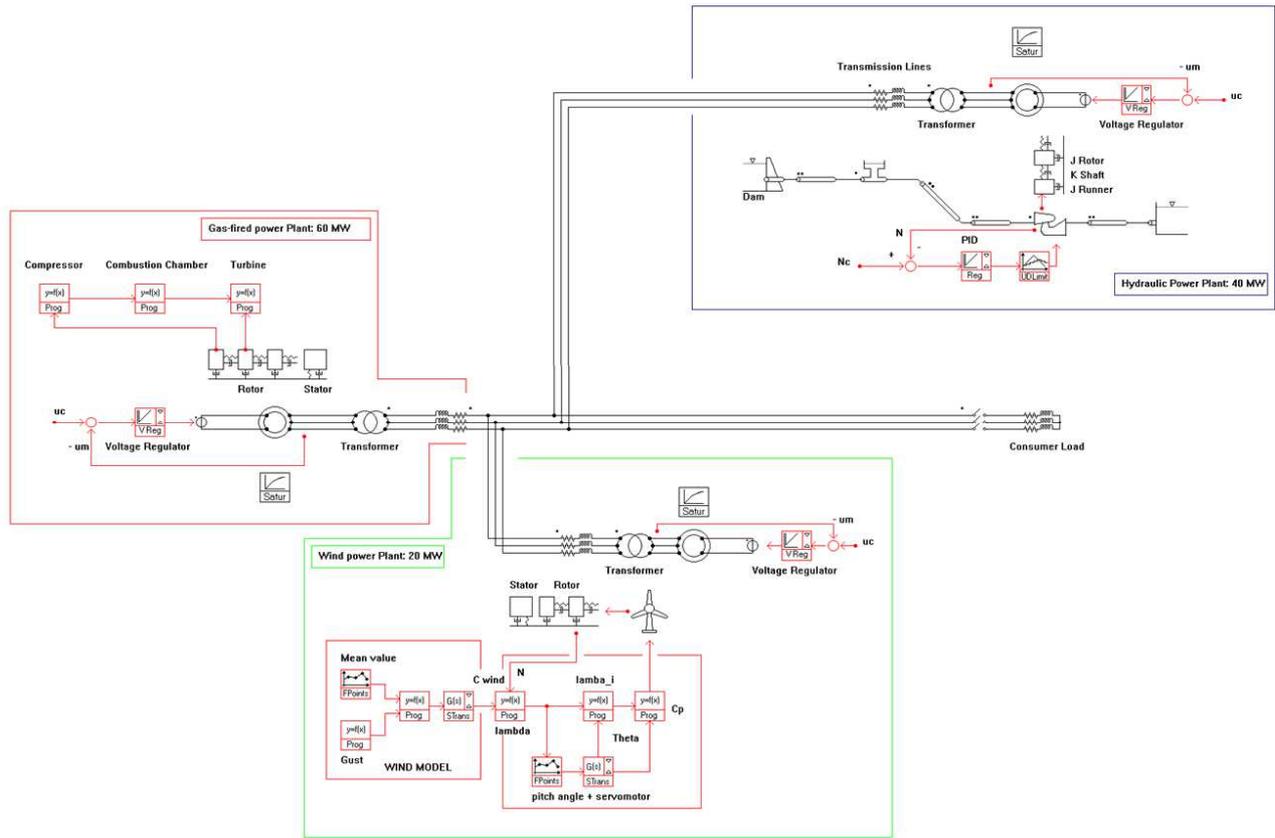**Figure 7**: Comparison of the adjustable load rates of four power plants [10]

Figure 8: Mixed Islanded Power Network SIMSEN model

For the analysis of the dynamic behavior of the mixed islanded power network, two different cases are considered and described:

- the first case consists of the compensation of the wind power variation due to wind velocity evolution,
- the second case is carried out for the power network subjected to a load rejection corresponding to the tripping of the 10 MW consumer.

In the first case, the wind velocity increases from a mean value of C_{inf} = 7.5 m/s to 15 m/s in 40 seconds. Then, after 220 seconds, the wind velocity decreases from a mean value of C_{inf} = 15 m/s to 7.5 m/s. The initial conditions of the power flow of the islanded power network are summarized in the table 4.

Table 4: Initial power flow before the wind increase

Element	Active Power P [MW]	Network Power level [%]	Power Flow
Wind farm	-2.94	2.54 %	Production
Gas-fired Power Plant	-77.30	66.76 %	Production
Hydropower Plant	-35.54	30.70 %	Production
Consumer Load	115.38	-	Consumption

The difference between production and consumption corresponds to the energy losses in both the transmission lines and the transformers. The Figure 9 describes the time history of the main parameter of the wind farm during the simulation. During the first 10 seconds, the wind velocity modeled by a PRBS fluctuates around a

mean value of 7.5 m/s. Then, it can be noticed that the wind increase induces output power increase and therefore the blade pitch angle is constantly adapted to maximize the power coefficient. However, after 40 seconds, the pitch angle is selected to generate the 2 MW output power limit of each wind turbine unit.
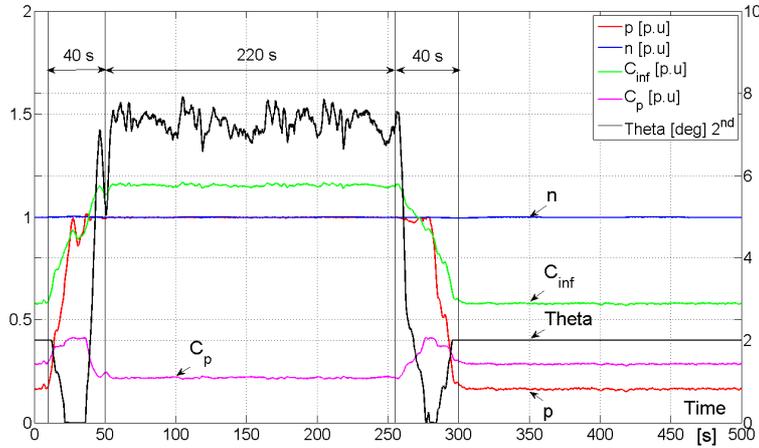

Figure 9: Time history of the wind farm parameters during the wind evolution

After 10 seconds, the wind power increase causes both an overproduction and a network frequency increase involving consequently an acceleration of different turbines. Thus, to ensure the stability of the islanded power network, the turbine speed governors stabilize the network frequency by closing the hydraulic guide vanes and by reducing the gas consumption of the gas-fired turbine and therefore the electrical output of the hydraulic and thermal parts are reduced. To better visualize the time history of generation and consumption on the grid, the Figures 10 and 11 show the time history of the active power of the hydro, gas-fired and wind power plants and of the consumer load during the wind evolution, respectively with a short and a long penstock.
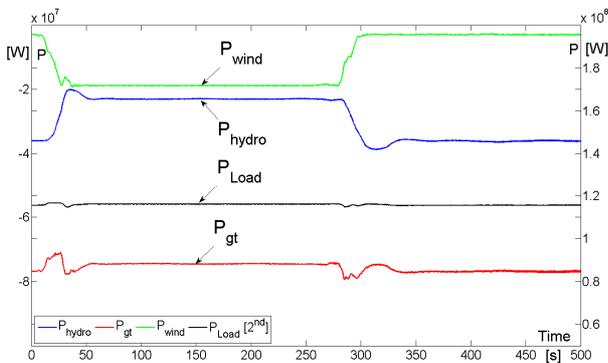

Figure 10: Transient behavior of the active power during the wind evolution for a short penstock
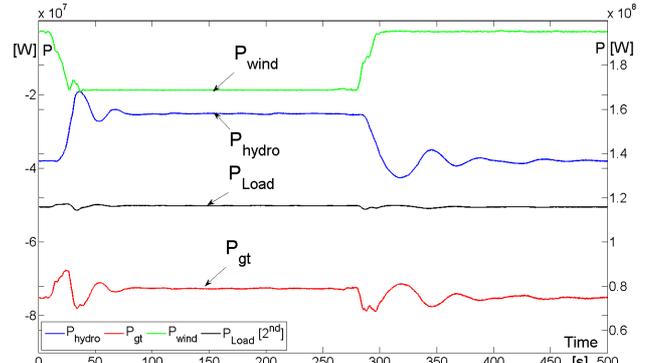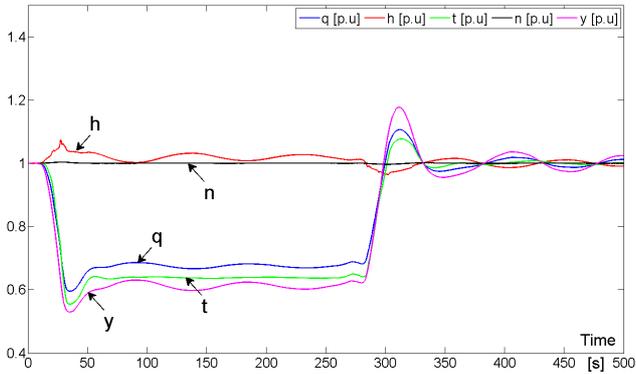
Figure 11: Transient behavior of the active power during the wind evolution for a long penstock

Overall, a long penstock emphasizes dynamic phenomena, such as waterhammer, surge tank water-level oscillation and turbine operation instabilities. Indeed, the increase of the penstock length causes an increase in the response time of the hydraulic system. Thus, when the turbine speed governors impose a closure of the guide vanes to reduce output power and therefore stabilize the network, the hydraulic system requires a period of 3.33 seconds before the torque begins to decrease. However, during this period, the power continues to increase and the regulator has to overreact to avoid too much change in the network frequency (see Figure 12).
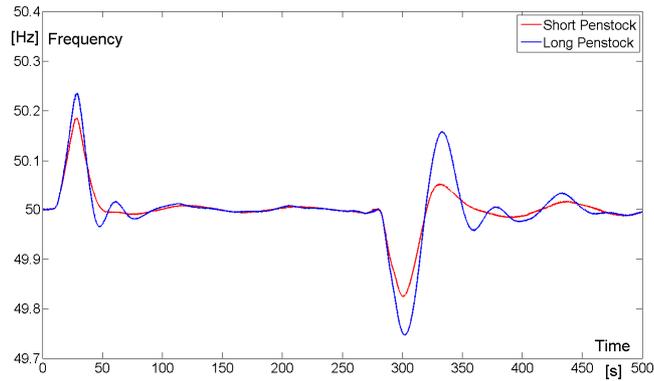
Figure 12: Time history of the network frequency for a long and a short penstock

Therefore, larger amplitudes of piezometric pressure *H*, discharge *Q* and power *P* appear that could lead to unstable behavior of the turbine; all these specific aspects are highlighted in the Figures 13 and 14.


Figure 13: Transient behavior of the hydraulic turbine parameters during the wind evolution for a short penstock
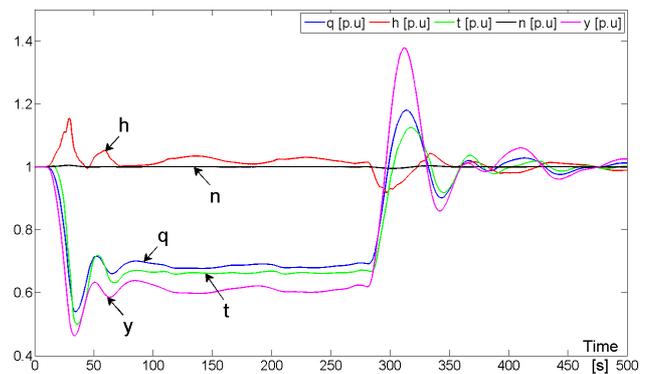
Figure 14: Transient behavior of the hydraulic turbine parameters during the wind evolution for a long penstock

More precisely, at time t = 15.8 seconds, the torque reaches its maximum value while the guide vane opening (GVO) decreases for a reaction time equal to 3.33 seconds (see Figure 15). This reaction time corresponds to the so-called reflection time of the penstock given by *2L/a*. This long reaction time causes an overpressure of 116.1% at the bottom of the penstock instead of 108.7% for a configuration with a short penstock. In addition, greater mass oscillations amplitudes between the surge tank and the dam appear and so a larger time is necessary to stabilize the system.
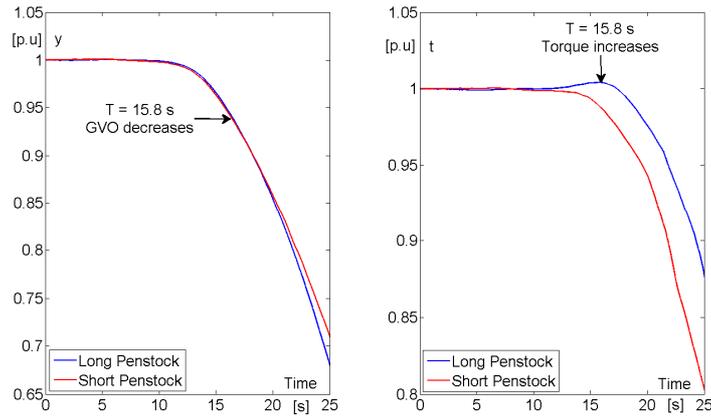
Figure 15: Time history of the guide vane opening *y* and the torque *T* for the hydraulic turbine

For the second case, the investigation is carried out for the power network subjected to a load rejection corresponding to the tripping of 10% of the consumer load. After 10 seconds, the power consumption drops instantaneously of 10 MW, changing the voltage on the network (see Figure 19). Therefore, the electromagnetic torque decreases causing an increase in the rotational speed of different synchronous machines. Thus, to avoid too large variations in network frequency, speed governors must act quickly and reduce mechanical torque. Initially, the hydraulic part compensates very quickly the power reduction imposed by the load rejection and the sharp drop in the thermal torque. Then, as the gas turbine performance is not very high at partial load, it will tend to stabilize around its nominal operating point forcing the hydraulic part to compensate for the gradual increase of production (see Figure 17).

Finally, as for the case of the wind variation, the system takes longer time to stabilize when the length of the penstock increases. Thus, a long penstock can lead to longer response time of the hydropower plant and reduces the power stability. Therefore, the hydraulic layout needs to be included in the stability assessment to study the nonlinear behavior of a mixed islanded power network.
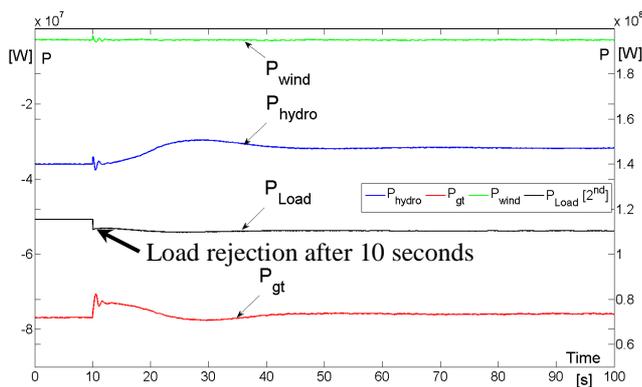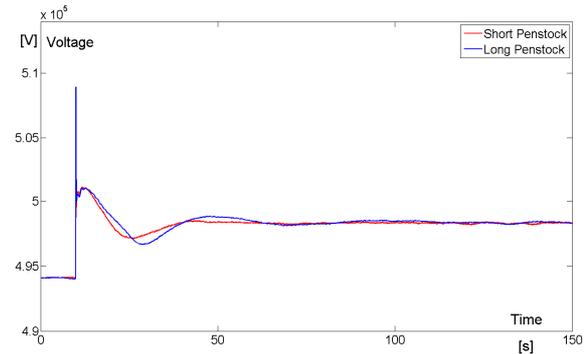

Figure 16: Transient behavior after a load rejection for a short penstock
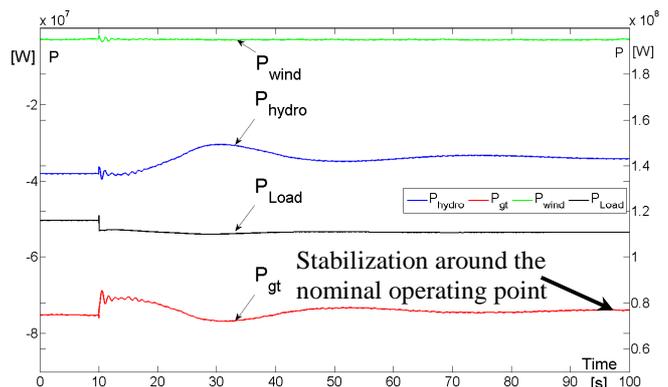
Figure 17: Transient behavior after a load rejection for a long penstock
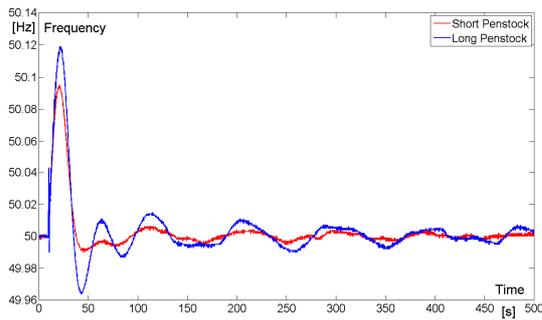
Figure 18: Time history of the network frequency for a long and a short penstock

Figure 19: Time history of the network voltage frequency for a long and a short penstock

CONCLUSION

The modeling, numerical simulations and stability analysis of an islanded power network comprising 40 MW of hydropower, 20 MW of wind power and 60 MW of gas-fired power plant were presented in this paper. The wind farm is modeled through an aggregated model approach of 10 wind turbines of 2 MW and comprises a stochastic model of wind evolution with wind gust. The model of gas-fired power plant includes an upstream rotating compressor coupled to a downstream turbine, and a combustion chamber in-between. To predict the performance of a gas turbine engine, both at design and off-design conditions, performance maps are integrated in the modeling.

The high dynamic performances of pumped storage plants are of highest interest for improving stability of mixed islanded power network, but require reliable simulation model of the entire power network for safety and optimization purposes. This study shows the evolution of the response time of the hydraulic part as function of the penstock length and highlights the influence of the hydraulic layout on the power system stability. Thus, a long penstock can lead to longer response time of the hydropower plant and reduces the power stability. Therefore, the hydraulic layout needs to be included in the stability assessment to study the nonlinear behavior of a mixed islanded power network.

NOMENCLATURE

A	Cross-section area [m^2]	H	Head [m]	y	Guide vanes opening [-]
a	Wave speed [m/s]	L	Hydraulic inductance [s^2/m^2]	T	Torque [Nm]
C	Hydraulic capacitance [m^2]	N	Rotational speed [1/min]	λ	Local loss coefficient [-]
C_{inf}	Wind velocity [m/s]	Q	Discharge [m^3/s]	μ	Dynamic viscosity [Pa·s]
D	Diameter [m]	R	Hydraulic resistance [s/m^2]	μ'	Expansion viscosity [Pa·s]
g	Gravity [m/s^2]	Re	Reynolds number [-]	v	Specific speed [-]
f	Frequency [Hz]	R_{ve}	Viscoelastic resistance [s/m^2]	ρ	Density [kg/m^3]

ACKNOWLEDGEMENTS

REFERENCES

[1] Wiik, J., Gjerde, J.O., Gjengedal, T. (2000), *Impacts from Large Scale Integration of Wind Farms into Weak Power Systems*, IEEE.

[2] Nicolet, C., Vaillant, Y., Kawkabani, B., Allenbach, P., Simond, J.-J., Avellan, F. (2008), *Pumped Storage Units to Stabilize Mixed Islanded Power Network: a Transient Analysis*, Proceedings of HYDRO, Ljubljana, Slovenia.

[3] Wylie, E .B. and Streeter, V.L. (1993), *Fluid transients in systems*, Prentice Hall, Englewood Cliffs, N.J.

[4] Nicolet, C., Alligné, S., Kawkabani, B., Koutnik, J., Simond, J.J. and Avellan, F., (2009), *Stability Study of Francis Pump-turbine at Runaway*, 3th IAHR International Meeting of the Workgroup on Cavitation and Dynamic Problems in Hydraulic Machinery and Systems.

[5] Nicolet C., Greiveldinger B., Hérou J.-J., Kawkabani B., Allenbach P., Simond J.-J., and Avellan F. (2007), *High-Order Modeling of Hydraulic Power Plant in Islanded Power Network*, IEEE Transactions on Power Systems, pp. 1870-1880.

[6] Slootweg, J. G. , De Haan, S. W. H., Polinder, H., Kling, W. L. (2003), *General model for representing variable speed wind turbines in power system dynamics simulations*, IEEE Transactions On Power Systems, Vol. 18, No. 1.

[7] Godfrey, K. (1991), *Design and application of multifrequency signals*, Computing & Control Engineering Journal, Vol. 2, Issue 4, pp. 187–195.

[8] Meherwan, Boyce, P. (2006), 2.0 Axial-Flow Compressors, *The Gas Turbine Handbook*, Houston NETL.

[9] Walsh, P.P, Fletcher, P. (2004), *Gas turbine performance*, Second Edition, Oxford Blackwell.

[10] Shin-ichi Inage (2009), *Prospects for Large-Scale Energy Storage in Decarbonised Power Grids*, International Energy Agency, OECD/IEA, Paris

[11] Keating, E., L., (1993), Applied Combustion, M. Dekker, Inc., New York.

[12] Turns S.R., (1996), An Introduction to Combustion, Mc Graw-Hill.